




Visualisation of H₂O₂ penetration through skin indicates importance to develop pathway-specific epidermal sensing

Skaidre Jankovskaja^{1,2} · Anaïs Labrousse³ · Léa Prévaut⁴ · Bo Holmqvist⁵ · Anders Brinte⁵ · Johan Engblom^{1,2} · Melinda Rezeli⁶ · György Marko-Varga⁶ · Tautgirdas Ruzgas^{1,2} 

Received: 30 July 2020 / Accepted: 1 November 2020 / Published online: 13 November 2020
© The Author(s) 2020

Abstract

Elevated amounts of reactive oxygen species (ROS) including hydrogen peroxide (H₂O₂) are observed in the epidermis in different skin disorders. Thus, epidermal sensing of H₂O₂ should be useful to monitor the progression of skin pathologies. We have evaluated epidermal sensing of H₂O₂ in vitro, by visualising H₂O₂ permeation through the skin. Skin membranes were mounted in Franz cells, and a suspension of Prussian white microparticles was deposited on the stratum corneum face of the skin. Upon H₂O₂ permeation, Prussian white was oxidised to Prussian blue, resulting in a pattern of blue dots. Comparison of skin surface images with the dot patterns revealed that about 74% of the blue dots were associated with hair shafts. The degree of the Prussian white to Prussian blue conversion strongly correlated with the reciprocal resistance of the skin membranes. Together, the results demonstrate that hair follicles are the major pathways of H₂O₂ transdermal penetration. The study recommends that the development of H₂O₂ monitoring on skin should aim for pathway-specific epidermal sensing, allowing micrometre resolution to detect and quantify this ROS biomarker at hair follicles.

Keywords Epidermal sensing · Hydrogen peroxide · Prussian blue · Hair follicles · Skin penetration

Introduction

Robust, non-invasive, or minimally invasive sensing on skin, often referred to as epidermal sensing, is one of the tools

Supplementary Information The online version contains supplementary material available at <https://doi.org/10.1007/s00604-020-04633-9>.

✉ Tautgirdas Ruzgas
tautgirdas.ruzgas@mau.se

- ¹ Department of Biomedical Science, Faculty of Health and Society, Malmö University, 205 06 Malmö, Sweden
- ² Biofilms - Research Center for Biointerfaces, Malmö University, 205 06 Malmö, Sweden
- ³ Department of Biological Engineering, Clermont Auvergne University, 63100 Aubiere, France
- ⁴ Faculty of Sciences, University of Montpellier, 34085 Montpellier, France
- ⁵ ImaGene-iT, Medicon Village, 223 81 Lund, Sweden
- ⁶ Clinical Protein Science & Imaging, Biomedical Centre, Department of Biomedical Engineering, Lund University, BMC D13, 221 84 Lund, Sweden

required to realise personalised healthcare, at point-of-care units or home self-monitoring. Epidermal sensing is carried out using epidermal electronics [1–3], microneedle patches [4], attachable, stretchable, biodegradable sensors [5], etc. These developments have strongly advanced sensing of molecular biomarkers by collecting and analysing sweat right on the skin [6]. To make this approach rapid and sensitive, sweating is usually stimulated, which might impose some burden on skin [7, 8].

Epidermal non-invasive sensing that does not rely on sweating or other types of skin interrogation is less developed [9]. In such cases, the most distal skin layer, the stratum corneum (SC), is considered a tough diffusional barrier [10–14]. The biomarkers are produced in viable epidermis and dermis layers, or become available due to blood microcirculation and partition in the interstitial fluid. In all these cases, the SC severely restricts biomarker leakage out on to the surface of the skin [15]. The full complexity of structural and functional features of the skin is still poorly accounted for in epidermal sensing [16], and e.g. sensing which does not rely on sweating or other types of skin interrogation is yet to benefit from the knowledge that different molecular biomarkers have preferred transdermal permeability pathways. Targeting

these pathways should improve epidermal sensing, e.g. in terms of lowered detection limits, faster detection, and better localisation of disordered skin areas.

Current technologies employed to make epidermal electronics and sensors allow manufacturing of nano- and micrometre-sized sensors, which could target specific transdermal biomarker permeability pathways, e.g. the hair follicular pathway [17, 18]. One of the restricting factors in developing pathway-specific epidermal sensing is that the permeability pathways are hard to visualise; hence, it will take some effort to convince the sensor and biosensor community that relying on these pathways is highly important for the development of superior epidermal sensing.

In this work, we show that transport of low molecular weight biomarkers, specifically H_2O_2 , across the SC has a specific dominant pathway. Since H_2O_2 is a biomarker of many inflammatory disorders, this discovery might be important for development of epidermal sensing of several common skin disorders. Specifically, increased epidermal H_2O_2 levels are reported for vitiligo [19], polymorphic light eruption [20], skin epithelioma [21], and xeroderma pigmentosum [22]. These skin disorders are associated with skin catalase deficiency, resulting in elevated topical H_2O_2 concentrations. For example, it has been reported that H_2O_2 can reach 1 mM in the epidermis of patients affected by vitiligo [19]. Hence, robust epidermal sensing of H_2O_2 could provide quantitative feedback in the management of anti-inflammatory measures, e.g. by justifying choice and dosage of medications, or selecting special anti-inflammatory diets. Anti-inflammatory diet components are often specific to a particular individual [23, 24], and to monitor effects of personalised anti-inflammatory diets, an efficient and reliable personalised “inflammation sensor” is needed. We hypothesise that robust, non-invasive epidermal monitoring of H_2O_2 could be one of the key components of an epidermal “inflammation sensor”, allowing a quantitative assessment of the efficacy of various anti-inflammatory measures that reduce reactive oxygen species (ROS) in the epidermis. In this work, we demonstrate that H_2O_2 permeates skin, or more strictly SC, predominantly through a specific hair follicle pathway. We also show that Prussian white (PW) microparticles, that are relatively stable towards O_2 , might serve as a possible sensing element for routine detection of H_2O_2 present on the skin surface. The sensing approach and the results of this work will encourage the development of pathway-specific epidermal sensing in general and, particularly, epidermal H_2O_2 sensing with micrometre resolution targeting the hair follicle pathway. To the best of our knowledge, this is the first time a predominant H_2O_2 transdermal pathway in skin is clearly demonstrated. This work exploits an *in vitro* Franz cell set-up that demonstrates that initial developments of epidermal sensing can be achieved without using animal models. The results obtained in this work are also relevant to improve methods of topical

application of H_2O_2 containing formulations for tissue oxygenation, which is one of the means to stimulate angiogenesis and healing of chronic wounds [25, 26].

Experimental

Materials

Sodium azide, potassium ferrocyanide ($\text{K}_4[\text{Fe}(\text{CN})_6]$), 30% HCl, FeCl_3 , soluble Prussian blue nanoparticles, ascorbic acid, and chloroform were obtained from Sigma-Aldrich (St. Louis, MO, USA). KCl, NaCl, Na_2HPO_4 , and KH_2PO_4 were purchased from Merck (Darmstadt, Germany). H_2O_2 35% w/w was obtained from Alfa Aesar (Kandel, Germany), and ferricyanide ($\text{K}_3\text{Fe}(\text{CN})_6$) from AppliChem, PanReac (Darmstadt, Germany). Phosphate buffer saline (PBS) was prepared using high-purity, 18.2 M Ω cm resistivity, Milli-Q water. PBS (pH 7.4) comprised 130.9 mM NaCl, 5.1 mM Na_2HPO_4 , and 1.5 mM KH_2PO_4 .

Preparation of skin membranes

Fresh porcine ears were acquired from a local abattoir and stored at -80°C . The ears are residuals from food preparation, and hence ethical permission is not required. To prepare skin membranes, defrosted pig ears were cleaned with cold water and cut into stripes with a scalpel. The stripes were shaved and 0.5-mm-thick skin membranes were obtained using a dermatome (TCM 3000 BL, Nouvag, Konstanz, Germany), and circular membranes (1.6 cm diameter) were punched out from the stripes. The video of skin membrane preparation is submitted as electronic supporting information. For preparing full-thickness skin membranes, a scalpel was used to remove all tissue attached to the ear cartilage (resulting in 3–4-mm-thick skin membranes).

Extraction of skin lipids: preparation of lipid-extracted skin membranes

In order to understand the role of the SC lipids in the H_2O_2 permeation mechanism, lipid-extracted skin membranes were prepared and used for H_2O_2 permeation studies, similarly to studies of intact skin. Lipid extraction from skin membranes was performed following a protocol published elsewhere [27]. Briefly, skin membranes were placed in 15 mL chloroform:methanol mixtures of the following compositions 2:1, 1:1, and 1:2 (v/v), and kept in each solution for 2 h. After that, the same procedure was repeated but the skin membranes were kept in each mixture for 30 min. Finally, skin membranes were left in methanol overnight, then rinsed with PBS and stored in a refrigerator (4°C) for a maximum of 3 days until use.

Monitoring of catalase activity in skin by using a skin-covered oxygen electrode

In skin membranes, catalase decomposes H_2O_2 to H_2O and O_2 ; and thus, the enzyme needs to be inhibited to allow PW/PB-based epidermal monitoring of H_2O_2 penetration through skin. Hence, the catalase activity and its inhibition in skin were monitored using an oxygen electrode [28]. Briefly, a skin membrane was firmly attached to the tip of the oxygen electrode by using a rubber O-ring and the assembly was inserted in an electrochemical cell filled with PBS, pH 7.4. After the baseline current of the electrode was stabilised, a defined amount of H_2O_2 was pipetted into the electrochemical cell (resulting in 4 mM H_2O_2 concentration) and the current response of the electrode was recorded (Fig. S1). When a steady-state current response was reached, the catalase inhibitor NaN_3 (14 mM) was added to the cell. The inhibition of catalase in skin returned the electrode current to the baseline current level. An additional portion of H_2O_2 (resulting in 8 mM) was added to ascertain that no further decomposition of H_2O_2 in skin membrane occurred. The latter result ascertained that complete inhibition of catalase in skin is achieved by 14 mM NaN_3 . The solution in the electrochemical cell was continuously mixed.

Measurement of the resistance of skin membranes mounted in Franz cells

To evaluate the skin membrane integrity and to appreciate H_2O_2 permeation pathways through skin, the electrical impedance of each skin membrane in the Franz cells was measured and the results were used to estimate the membrane resistance. Electrical impedance spectroscopy measurements were conducted with a skin membrane mounted in a Franz cell (PermeGear Inc.; opening diameter 0.9 cm, lower chamber volume 6 mL) equipped with four electrodes; see Fig. S2 [29]. The impedance spectroscopy measurements in the 1-Hz to 1-MHz frequency range, an applied DC voltage of 0 V, and an AC voltage amplitude of 10 mV were carried out by using a potentiostat from Ivium Technologies (Eindhoven, the Netherlands). The skin resistance was determined by fitting the impedance spectroscopy data to an equivalent circuit composed of solution resistance connected in series with skin membrane impedance (Fig. S2). Skin membrane impedance comprised parallel connection of skin membrane resistance (R_{mem}) and constant phase element (CPE) (equivalent of capacitor). The fitting was done using Ivium software.

Synthesis and characterisation of Prussian white particles

Air-stable (resistant to oxidation by O_2 in air) PW particles were synthesised hydrothermally following a previously reported

protocol [30]. Briefly, 100 mL of a 30 mM $\text{K}_4[\text{Fe}(\text{CN})_6]$ solution in water was degassed by mixing and applying vacuum for 20 min. The solution was then transferred to a Teflon-lined stainless steel autoclave (Toption Group Co., Limited, Hecheng, China) and was additionally purged with nitrogen to remove dissolved oxygen. The autoclave was sealed and maintained at 160 °C for 48 h; when room temperature was reached, the supernatant was discarded and the white particulate precipitate was collected. The particles were washed several times with 0.1 M KCl in distilled water and acetone, and finally dried under vacuum for 12 h. Commercially available PB nanoparticles were reduced to PW by washing them with saturated ascorbic acid solution in 0.1 M KCl.

The morphology of the PW particles was assessed by a scanning electron microscope (SEM; EVO LS10, Zeiss, Germany), equipped with a LaB6 filament. Briefly, different dilutions of the particles were drop-casted on Leit carbon tapes (Agar Scientific) and left to dry. Prior to SEM measurements, the samples were covered with gold, layer thickness < 10 nm, using an Auto Agar Sputter Coater (Agar Scientific, Cambridge, UK): parameters $I = 30$ mA, $t = 40$ s, and $P = 0.08$ mbar. Images were recorded in high vacuum mode, using a secondary electron detector, 15 kV accelerating voltage, and 50 pA probe current.

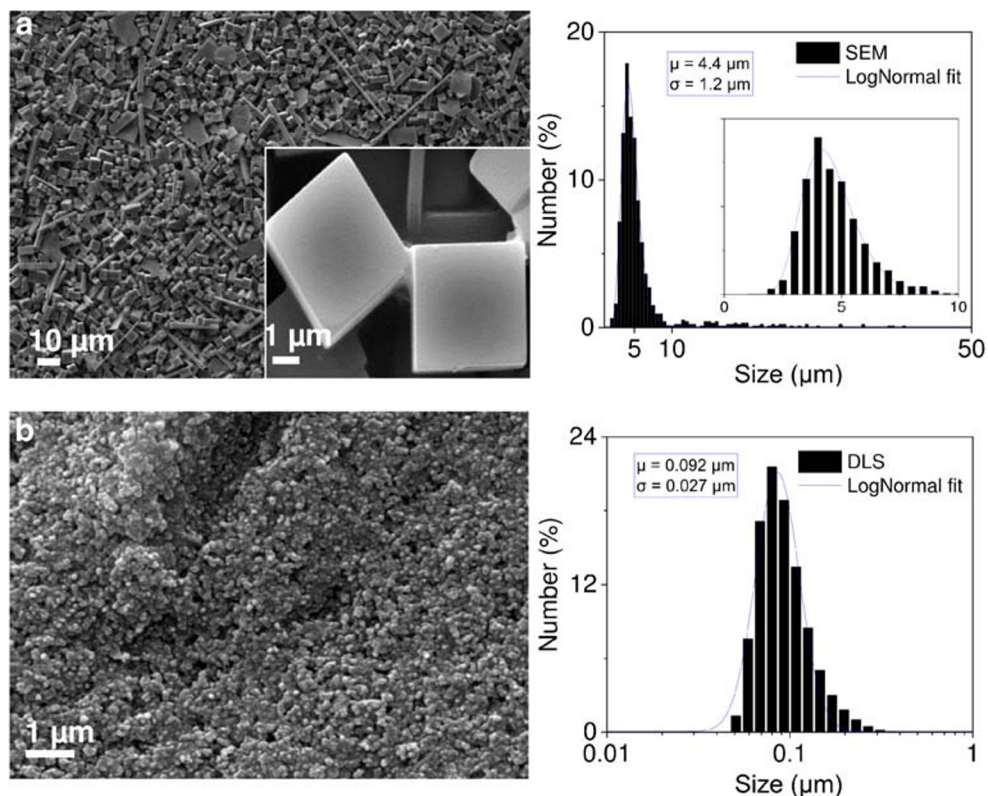
SEM images of PW particles (Fig. 1a) were analysed with the ImageJ software to obtain the size distribution of the particles. Particle size was defined as the longest dimension measured along the PW particle. The average size of the particles was estimated after measuring the size of 990 individual particles and fitting the data to the LogNormal distribution model. Details regarding evaluation of PW particle size and shape can be found in the supporting information (Fig. S3 and Table S1).

The size of commercially available PB particles was measured by dynamic light scattering (DLS, Malvern Zetasizer Ultra, Malvern, Worcestershire, UK). The samples were prepared in deionised water. The average particle size equalled 164.7 ± 4.5 nm ($n = 4$, measurements using different dilutions and intensity weighting). To be able to compare commercially available PB particles with the synthesised PW particles, the PB size distribution determined by DLS was number-weighted and expressed in terms of number percent. The size distribution of PB particles was fitted to the LogNormal distribution model.

Epidermal monitoring of H_2O_2 penetration through skin by imaging PW particles on skin

PW particles were deposited on the surface of the membrane (Scheme 1). Dermatomed (thickness 0.5 mm) or full-thickness (thickness 3–4 mm) skins were mounted in vertical-type Franz cells with the 6-mL lower chamber (serving as donor) filled with PBS, pH 7.4, 14 mM NaN_3 (20 mM for full-thickness

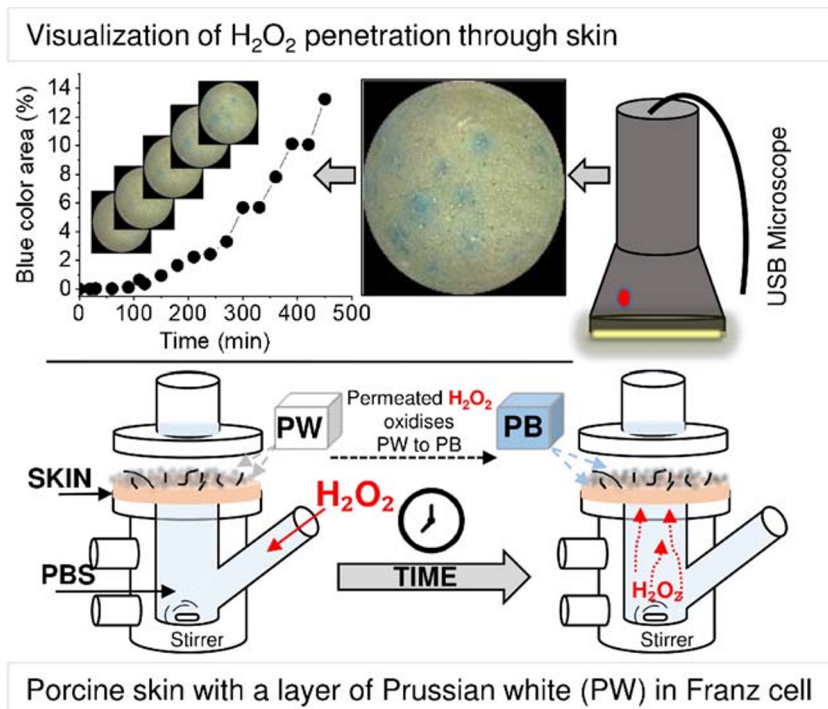
Fig. 1 Scanning electron micrographs and particle size histograms of PW particles used to develop epidermal sensing of H_2O_2 . Curves are fitted to LogNormal size distributions. **a** O_2 -stable PW microparticles, mainly composed of cube-like particles. **b** Commercially available PB nanoparticles, which have been reduced to PW by washing them with ascorbic acid. These PW nanoparticles exhibited high sensitivity to O_2 (i.e. they became blue in few minutes when exposed to air). μ and σ stand for arithmetic mean particle size and standard deviation



skin). The top chamber was filled with an identical solution (0.6 mL). The dermal skin side faced the lower chamber. Skins were left to equilibrate for 30 min in the Franz cell, and the electrical impedance was measured as described above. After equilibration, the PBS solution in the top

chamber (stratum corneum plane of the skin) was removed and the skin surface structure was imaged using a digital USB microscope ($\times 1000$, China). Upon emptying of the top chamber, the Franz cell position remained fixed throughout the experiment. Two milligrammes of PW suspended in

Scheme 1 Schematic presentation of a skin membrane enclosed in a Franz cell. The skin was covered by PW microparticles. The lower chamber was filled with PBS containing H_2O_2 and 14 mM NaN_3 . With time, the H_2O_2 permeated the skin membrane and converted PW to PB. The development of blue colour was photographed using a USB microscope. The microscopy images revealed dominant H_2O_2 permeability pathways and the development rate of the blue area could be estimated



200 μL of 0.1 M KCl was spread on the skin surface and a defined amount of H_2O_2 was pipetted into the lower chamber of the Franz cell. The resulting solution (4 mM H_2O_2) in the lower chamber was continuously agitated using a magnetic stirrer. Directly after the H_2O_2 introduction, the skin surface with deposited PW particles was imaged and the photo was assigned as the skin/PW image at time 0 (0 min). The images were then recorded at regular time points. To overcome the disturbance from external light, an illumination ring (Optica Microscopes, Ponteranica, Italy) was mounted on the microscope and the entire Franz cell–microscope set-up was shielded from external light by a cardboard box.

Penetration experiments with a lower H_2O_2 concentration (0.5 mM) were supplemented by an external peristaltic pump (LabKemi, Sweden) connected to the lower chamber of the Franz cell. This allowed refreshing the PBS buffer/0.5 mM H_2O_2 each hour, to avoid possible degradation of H_2O_2 . All measurements were conducted at room temperature, 22 °C.

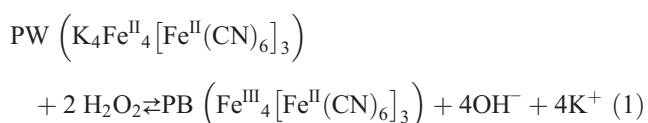
Image analysis

The ImageJ software (v. 1.51j8, Java 1.8.0_112, 64-bit) in combination with an adapted script (provided by ImaGeniT, Lund, Sweden) was used for image processing. Briefly, skin surface images were cropped and converted to cyan, magenta, yellow, and black (CMYK) images. Then, cyan images were compared with an original photographic image; the B&W threshold was adjusted for each image (the threshold for different images varied slightly).

Results

Franz cell-based set-up for assessing epidermal sensing of H_2O_2

Taking into account that Prussian blue (PB) is highly biocompatible and nontoxic (an oral intake of 1–10 g/day of PB is recommended after exposure to radioactive caesium) [31, 32], we considered the possibility to monitor H_2O_2 on the skin surface using the Prussian white–Prussian blue redox couple [33]. Equation 1 describes the PW/PB redox conversion in reaction with H_2O_2 .



H_2O_2 , in the redox reaction (Eq. 1), is an oxidant that converts PW ($\text{K}_4\text{Fe}^{\text{II}}_4[\text{Fe}^{\text{II}}(\text{CN})_6]_3$) to PB ($\text{Fe}^{\text{III}}_4[\text{Fe}^{\text{II}}(\text{CN})_6]_3$), and consequently the PW crystal colour changes from white to blue [34]. Hence, PW microcrystals were deposited on skin

membrane surfaces in an attempt to verify if the conversion to PB can be used to monitor H_2O_2 penetration through skin membranes. This *in vitro* approach can be considered as a good model for assessing epidermal sensing of H_2O_2 ; we consider the approach as being a necessary step before testing the sensing *in vivo* using living animals or humans.

The experimental set-up comprised a skin membrane placed in a Franz cell (Scheme 1). The skin membrane was covered with a layer of PW crystals (3.1 mg cm^{-2}). H_2O_2 permeability through skin resulted in PW turning blue. The colour change was visualised by a USB microscope. The results revealed that PW microparticles could be adopted as a sensing material for monitoring H_2O_2 penetration through skin. The observed H_2O_2 permeability was rationalised by considering transdermal penetration pathway theory [35].

Inhibition of catalase activity in skin

In healthy skin, catalase, the main H_2O_2 detoxifying enzyme, converts H_2O_2 into water and oxygen [36]. In *in vivo* situations, when the skin is affected by various skin disorders (vitiligo [19], xeroderma pigmentosum [22] etc.), catalase activity is downregulated resulting in elevated H_2O_2 concentrations in the epidermis. Working with skin *in vitro* and aiming to monitor H_2O_2 presence on the skin surface, or to monitor H_2O_2 transdermal penetration, the skin catalase is an obvious problem since it converts H_2O_2 to H_2O and O_2 . Therefore, to assure H_2O_2 penetration, skin catalase in skin membranes has been inhibited. The inhibition process was confirmed by using skin membranes firmly attached to oxygen electrodes. The set-up is known as skin-covered oxygen electrode (SCOPE), which measures O_2 liberated by skin catalase when the electrode is exposed to a solution of H_2O_2 [25, 28, 37]. Figure S1 in the supporting information provides an example of the current response when the SCOPE is exposed to H_2O_2 in the absence and in the presence of a catalase inhibitor, specifically sodium azide, NaN_3 . Amperometric measurements with the SCOPE did show that 14 mM of NaN_3 is sufficient to inhibit more than 90% of skin catalase. Sufficient NaN_3 amounts were thus always present in solutions of the Franz cell experiments.

Synthesis and choice of Prussian white particles

Due to the potent diffusional barrier of the SC, permeability assays using Franz cells are usually conducted over several hours and it is expected that epidermal H_2O_2 monitoring in clinical situations might be equally time demanding. Hence, it is an absolute requirement that PW particles are stable against oxidation by ambient O_2 and O_2 dissolved in solution. PW oxidation by O_2 is rarely reported, but depending on the particle structure, O_2 can oxidise PW to PB in a few minutes or months. Various synthesis trials showed (data not shown) that

micrometre-sized PW particles are more O₂-stable. Specifically, we found that PW particles with an average size of 4.4 μm ± 1.2 μm (mean ± SD) (Fig. 1a) are O₂-stable; when put in a closed Ependorf tube, or re-suspended in KCl solution, they can be kept in the PW state for weeks. Meanwhile, sub-micrometre particles, i.e. with an average size of 0.092 μm ± 0.027 μm (mean ± SD) (Fig. 1b), were unacceptably sensitive to O₂, i.e. PW nanoparticles were converted to PB in a few minutes or hours.

These visual observations of PW particle stability towards O₂ can be supported by the results of Hu and co-workers (2011), who performed Mössbauer spectroscopy measurements on the PW particles synthesised by the same synthesis protocol that was used in our study. In their work, Mössbauer spectra of PW particles were unchanged after exposure to air for 2 months [30]. The spectra show that there are just two absorption peaks, characteristic of the reduced form of iron, Fe^{II}, indicating that PW of this size is stable against oxidation by O₂ in air.

The size stability of our PW particles over time was assessed using light microscopy. A few PW particles were re-suspended in KCl solution and were imaged every day for 5 days. With no apparent change in shape and size of the particles, it was concluded that the PW particles are stable for at least 5 days in KCl solution (Fig. S4 and Table S2). In addition, SEM images of PW particles taken a year after synthesis did not show any obvious differences regarding size and/or shape, compared to the size and shape of the particles assessed by SEM directly (a few days) after synthesis (data not shown).

PW/PB-based epidermal monitoring of H₂O₂ penetration through skin membranes

Colorimetric monitoring of transdermal H₂O₂ penetration was done by performing Franz cell permeation assays; vide supra, Scheme 1. The eventual settling composed of the PW micro-particle layer on a skin membrane with a 3.1 mg cm⁻² PW coverage. The skin membrane was periodically photographed, which allowed monitoring of PW oxidation to PB due to the transdermal permeation of H₂O₂ from the dermal side of skin membrane onto its SC surface (Fig. 2).

The analysis of the images (Fig. 2) was carried out by converting the photographic skin surface images into cyan images and, subsequently estimating the percentage of the cyan colour area at the particular time point of the permeability experiments. As can be seen from Fig. 2a and c, the blue area increases over time, of H₂O₂ penetration experiment, albeit differently for five different skin membranes (the reasons are explained in the next paragraph). Control experiments with no addition of H₂O₂ into the Franz cells showed no PW oxidation to PB over 24 h.

As can be judged from longer measurements (> 24 h, Fig. 2c), most of the skin membranes approached 100% blue coverage indicating that PW particles were sufficiently evenly distributed over the entire surface of the skin membranes. This is particularly clear from the blue colour development of lipid-extracted skin membranes (Fig. 2b and d).

Prior to H₂O₂ penetration experiments, all skin membrane samples were evaluated by measuring the membrane electrical impedance, in order to estimate membrane resistance (R_{mem}) values; an example of impedance data is shown in Fig. S2. Impedance measurements show that the resistance of untreated skin membranes, with a surface area of 0.64 cm², was 12.6 kΩ ± 7.3 kΩ (mean ± SD, n = 5) on average, while lipid-extracted skins had an average resistance value of 0.20 kΩ ± 0.02 kΩ (mean ± SD, n = 5). As can be seen from Fig. 3a, the rate of blue colour development differs from membrane to membrane. The development of the blue area on skin correlated to the reciprocal resistance of the membrane (Fig. 3a, inset). For example, the blue colour fraction of the area, measured at the 4th hour (Fig. 3a, inset), was 5.9% for the membrane with R_{mem} = 6.4 kΩ, 3.4% for R_{mem} = 8.1 kΩ, 2.4% for R_{mem} = 9.5 kΩ, 1.2% for R_{mem} = 14.9 kΩ, and 0.04% for R_{mem} = 24.3 kΩ, respectively. The observed correlation between H₂O₂ permeation (i.e. blue colour development) across the skin membrane and reciprocal of skin resistance indicates that H₂O₂ penetrates the skin through the same pathway as hydrated ions. Additionally, the blue colour development kinetics on non-treated skin membranes, e.g. median resistance membranes (Fig. 3b, R_{mem} = 9.5 kΩ), was attenuated compared to lipid extracted membranes (Fig. 3c, R_{mem} = 0.2 kΩ). On lipid-extracted skin, more than 90% of the image did turn blue in less than 30 min (Fig. 3c). This confirms that SC lipid structures are the main barrier for permeability of hydrophilic biomarkers.

Assessment of the mechanism of transdermal H₂O₂ penetration by epidermal sensing

During the PW-based epidermal monitoring of H₂O₂, a development of dot-like pattern of blue colour was always observed. This was conspicuously clear at the beginning (time < 4 h) of the experiments (Fig. 2a). This indicated that H₂O₂ permeates through skin appendages, and probably preferably through hair follicles. To check this hypothesis, all visible hair shafts were counted prior to the deposition of PW particles on skin. Then, skin images with marked hairs were overlaid with the blue (cyan) images (Fig. 4) and the percentage of blue colour associated with hair shafts was calculated (Table S3). Keeping the difficulty to recognise all hairs from photographic images in mind, the results are surprisingly consistent; 74% ± 7% (mean ± SD, n = 5) of the blue dots are associated with hair shafts (Table S3).

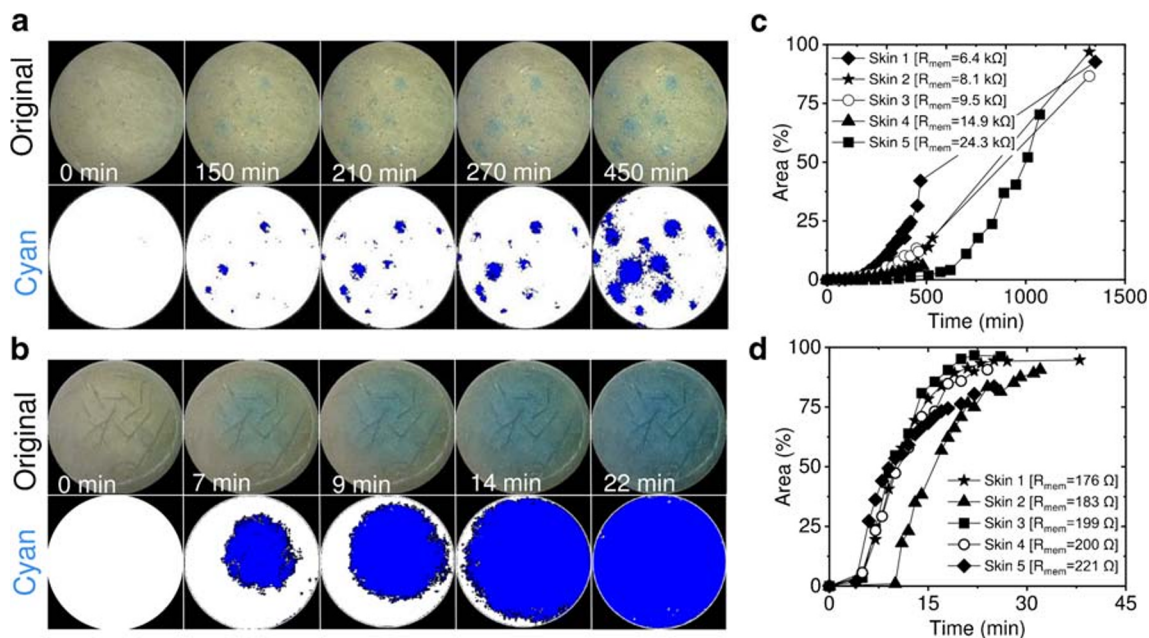


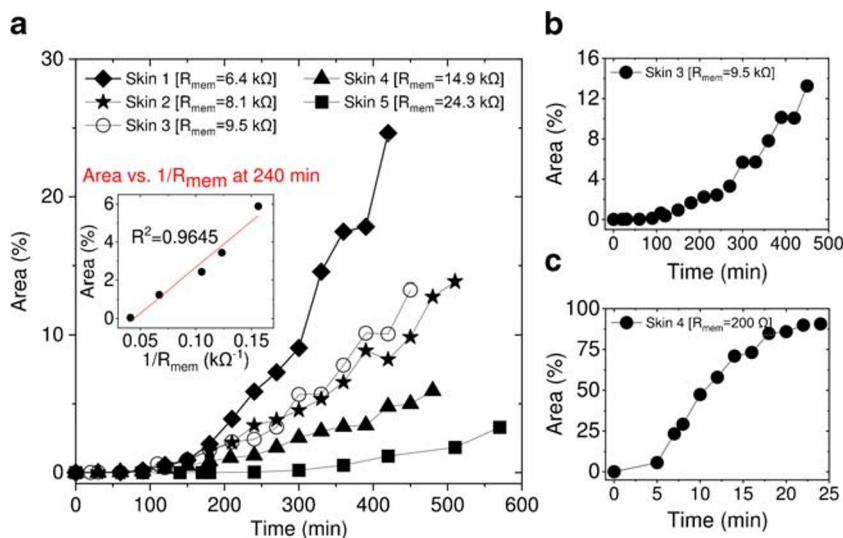
Fig. 2 Visualisation of H₂O₂ skin membrane penetration by imaging the development of blue colour in the PW particle layer situated on the SC side of the skin membrane. The original photographic and corresponding cyan images are presented at certain time points after initiation of H₂O₂ penetration. Time 0 corresponds to the moment when the concentration of H₂O₂ in the lower Franz cell chamber was raised to 4 mM. Images taken for **a** unprocessed/natural skin membrane and **b** skin membrane after lipid

extraction. The blue colour development is due to skin penetration of H₂O₂ and conversion of PW to PB (reaction Eq. 1). The images are taken by USB microscope. **c, d** Area % vs. time plots reflect an increase of the blue colour fraction with time due to PW conversion to PB on skin for cases of **c** unprocessed and **d** lipid-extracted skin, respectively. 100% area corresponds to the geometric area of the skin membrane since the entire surface became blue at the end of the experiment

After membrane lipid extraction, the dot features of the blue colour were not observed (Fig. 2b); rather, the entire membrane area became blue, suggesting a complete disruption of H₂O₂ permeation pathways. These results indicate that hair follicles do not share the overall SC barrier features, and that is probably the reason why hair follicles act as dominant pathways of transdermal penetration of hydrophilic biomarkers such as H₂O₂. However, based on our calculations

(Table S3), only 55% ± 22% (mean ± SD, n = 5) of all hair shafts were associated with blue colour development. The notable variation and relatively low fraction of hair follicles associated with facile H₂O₂ penetration (55%) might be due to structure and growth cycle differences of a particular hair. It is known that approximately 26% of the hair follicles present in human forearm skin are inactive; i.e. they do not excrete sebum and are filled with a corneocyte plug which restricts

Fig. 3 Development of the blue colour, area (%), on the skin surface due to H₂O₂ skin permeation. **a** The plot and the insert show that the development of the blue area strongly correlates with the reciprocal resistance of skin membranes (R_{mem}). **b, c** Rate differences (compare time axes) of blue colour development on **b** untreated/natural and **c** lipid-extracted skin membranes



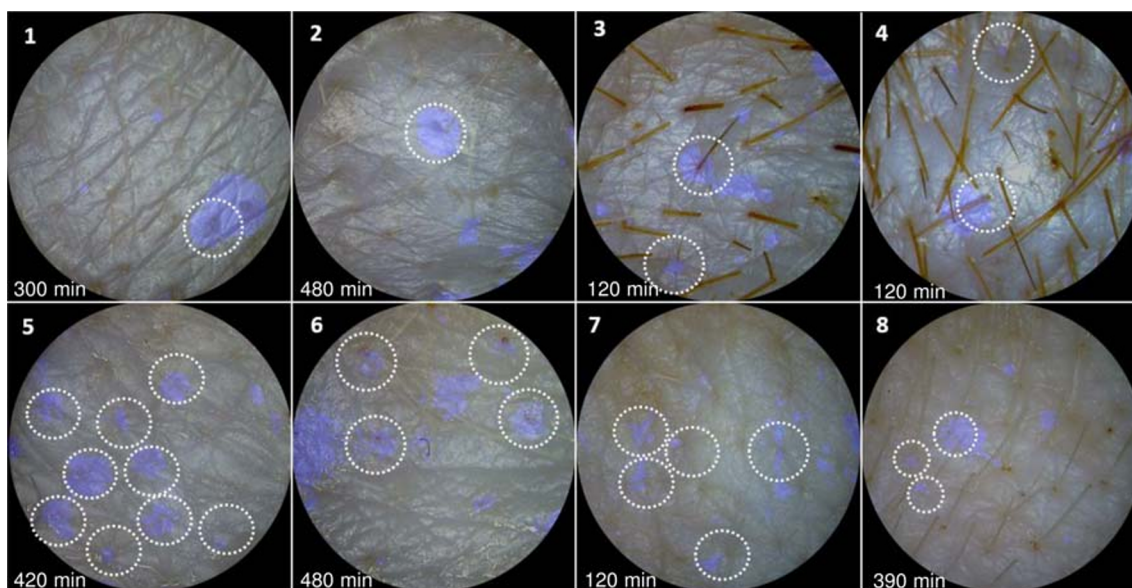


Fig. 4 Overlay of skin surface images and blue (cyan) dot patterns developed in the PW layer on skin membranes during H_2O_2 permeability assays. Dashed circles mark identified hair shafts surrounded by oxidised PW, i.e. PB. The number on each sub-figure (1–8) indicates different skin membranes used for H_2O_2 permeability experiments. 1–3, 5, and 6 skin images are taken from H_2O_2 permeability experiments performed on split thickness (0.5-mm thickness) skin membranes when the concentration of

H_2O_2 in the lower Franz cell chamber was raised to 4 mM. Skin image 4 and 7 is taken from the permeability experiment performed on split-thickness skin exposed to 0.5 mM H_2O_2 . Skin image 8 is from a permeability experiment performed on a full-thickness skin membrane, exposed to 4 mM H_2O_2 . The skin surface images were captured at the time points indicated on the image

penetration of both hydrophilic and hydrophobic molecules [38]. The study however refers to human skin, but it is assumed that similar features are shared by porcine skin.

Validation of the major H_2O_2 penetration pathway using full-thickness skin membranes

To validate that hair follicles are the dominant transdermal H_2O_2 penetration pathways, additional experiments were carried out. First, epidermal monitoring of the permeation from a lower, more physiologically relevant concentration (0.5 mM) of H_2O_2 was evaluated (Fig. 5a). The results (Fig. 5a; $R_{\text{mem}} = 6.5 \text{ k}\Omega$) indicate slower PW particle oxidation, compared to measurements on skin with similar resistance but with eight times higher H_2O_2 concentration (compared to Fig. 3a, skin1 with similar $R_{\text{mem}} = 6.4 \text{ k}\Omega$). When the skin membrane was exposed to 0.5 mM H_2O_2 , after 8 h only 4.6% of the area was coloured blue (Fig. 5a), whereas in skin with similar resistance exposed to 4 mM of H_2O_2 , 24.6% of the area was coloured after a similar time, i.e. 7 h (Fig. 3a). Again, the blue dot pattern is obvious even with the lower concentration of H_2O_2 .

Additionally, since hair follicles can be lodged up to 4 mm deep inside the skin [39] and our dermatomed (split thickness) membranes are 500 μm thick, it can be suspected that the dot pattern observed may be due to cutting of deeper grown hair follicles. To ensure that the blue dot pattern is not an artefact, full-thickness skin membranes were prepared and experiments identical to those of dermatomed skin were performed (Fig.

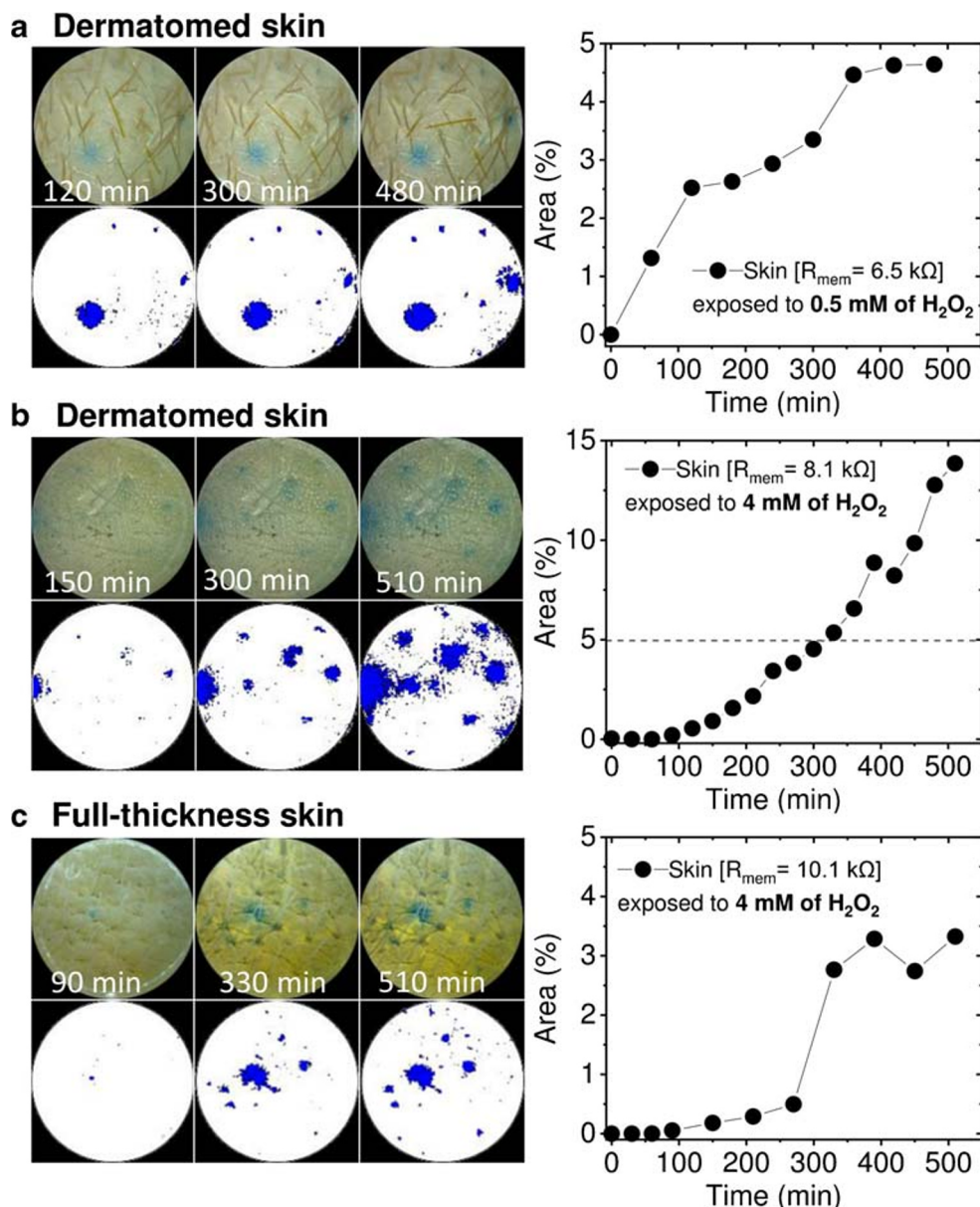
5c). As shown in Fig. 5, regardless of whether dermatomed or full-thickness skin was employed, the same dot-like PW oxidation to PB pattern due to H_2O_2 transdermal permeation was observed. It can also be noticed that the first few visible blue dots appear 1–2 h after the start of the H_2O_2 permeability assay (Figs. 2 and 5).

Discussion

Obstacles of PW/PB-based epidermal monitoring of H_2O_2 on skin

To establish image analysis-based epidermal monitoring of H_2O_2 permeation across skin membranes, a PW particle suspension was applied directly on the skin membrane secured in a Franz cell (Scheme 1). The idea draws on the insight that PW microparticles in contact with H_2O_2 turn blue, i.e. PW becomes blue PB (Eq. 1). Given that various skin ailments and disorders are characterised by H_2O_2 production, a monitoring approach based on an easily detected colour change seemed obvious. However, two critical obstacles had to be circumvented. Firstly, skin is abundant with catalase; thus, to observe H_2O_2 penetration through skin, skin catalase needs to be inhibited. Secondly, it appeared that O_2 , present in air or as a solute, oxidises PW to PB. Though PW/PB-based H_2O_2 sensing is broadly used, the reactivity of PW with O_2 is rarely reported [40–43].

Fig. 5 Epidermal monitoring of H_2O_2 penetration through skin membranes (Scheme 1). Skin membrane (0.5-mm thick) exposed to **a** 0.5 mM and **b** 4 mM H_2O_2 . **c** Blue colour development on full-thickness skin (approx. 4-mm thick) during permeability of H_2O_2 from 4 mM solution



High abundance of catalase in skin has been clearly shown by skin-covered oxygen electrode measurements [28]. Catalase in skin remains active after prolonged (more than a year) storage of skin membranes at -20°C (unpublished data); hence, for performing H_2O_2 permeability experiments, skin catalase must be inhibited. We found that 14 mM NaN_3 is sufficient to inhibit catalase in skin (Fig. S1). Thus, appropriate amounts of NaN_3 were always present in solutions used for H_2O_2 permeation measurements.

Another observation made during our studies was that the PW/PB redox pair has a considerable sensitivity to O_2 . This fact is often neglected since sensors for H_2O_2 based on PW/PB are usually tested for several minutes only. However, transdermal permeation might take hours; the long time is needed for molecules (especially hydrophilic) to cross the

barrier maintained by the SC. Despite the fact that many research articles [44, 45] and detailed reviews [34, 45] focus on PB synthesis, only a few reports can be found that address synthesis of PW with reduced reactivity towards O_2 [30, 46]. The method proposed by Hu and Jiang [30] yielded PW cube-like microparticles (Fig. 1a), and satisfactory stability against oxidation by O_2 ; the PW microparticles stay white (i.e. white-grey) for more than 2 months when kept in a closed Eppendorf tube. Based on experience with different synthetic routes, it was concluded that smaller particles ($<0.2 \mu\text{m}$) are highly prone to oxidation by O_2 in air or solution, and are thus not suitable for optical epidermal sensing of H_2O_2 . Thus, micrometre-sized PW particles were used to develop epidermal H_2O_2 sensing and to visualise pathways of H_2O_2 penetration through skin.

Epidermal monitoring of biomarkers can benefit from skin resistance measurements

Epidermal monitoring of transdermal H_2O_2 penetration carried out in this work relied on (i) skin membranes mounted in Franz cells; (ii) deposition of a H_2O_2 -sensitive, but O_2 -insensitive PW microparticle layer on the SC face of skin membranes; (iii) recording the blue colour development of the dispersed PW microparticles, due to reaction with permeated H_2O_2 ; and (iv) complementing the colour-based assay with skin integrity measurements using electrical impedance spectroscopy. Repeated epidermal monitoring of H_2O_2 with different skin samples revealed that it takes 3 to 10 h until about 4% of the skin area is covered with blue colour (Fig. 3a). The extended time required for H_2O_2 penetration confirms that the SC is a potent diffusional barrier for the hydrophilic biomarkers. The results further suggest that clinically relevant epidermal sensing of H_2O_2 might require robust hour-long skin monitoring. It is important to notice that reciprocal of skin resistance, $1/R_{\text{mem}}$, i.e. conductance, correlated linearly with the blue area development rate (Fig. 3a, inset). The simultaneous R_{mem} and H_2O_2 permeability measurements add to the understanding of the differences observed in H_2O_2 penetration through different skins and help explain the biological variability of the SC biobarrier. Summarising, it can be concluded that if complemented with simultaneous skin impedance measurements, epidermal sensing of biomarkers, as in this case H_2O_2 , should significantly improve analysis robustness and result interpretation. We believe that such a combination has not yet been realised in epidermal sensing.

Epidermal monitoring of H_2O_2 revealed hair follicles as the dominant H_2O_2 permeability pathways through skin

In a simplified view of permeation across a skin barrier, at least two separate routes of penetration can be distinguished. First, skin appendages comprised sweat ducts and hair follicles, and, second, intercellular and transcellular penetration pathways [47–49]. The scientific community questions if skin appendages have an impact on transdermal permeation, owing to the minute skin surface fraction occupied by the appendages, i.e. approx. 0.1% of the total skin surface [49]. In addition, the molecular details of how hair follicles and appendages allow higher permeability remain unclear. Some researchers state that due to the sebum present in active hair follicles, this route facilitates lipophilic molecule penetration [50, 51]. Another group of scientists suggests that hair follicles are the dominant transdermal penetration pathways for hydrophilic molecules [52–54]. The last rationale was recently pointed out in epidermal measurements of interstitial glucose [17]. The researchers compared glucose detection on a skin area with high hair follicle density (34 hairs/cm²) vs. an area

with low density of hair follicles (6 hairs/cm²). They found that the follicle-dense skin allowed almost nine times higher flux of glucose if compared with the flux across the follicle-poor area of the porcine skin [17].

Our results show that H_2O_2 penetration through skin generates a blue colour dot-like pattern in the H_2O_2 -sensitive PW particle layer deposited on the surface of skin membranes (Figs. 2, 4, and 5). The pattern strongly supports the appendage route as being the dominant transdermal H_2O_2 penetration pathway. Overlaying of skin images, recorded before deposition of PW layer (Fig. 4), with the blue colour dot images of the same skin covered with PW during H_2O_2 penetration experiments, shows that a majority of the blue dots develop around the hair shafts (74% ± 7%, Table S3). This strongly suggests that hair follicles are the dominant H_2O_2 penetration pathways. A substantial number of blue colour dots (≤ 26%) appeared at skin sections without visible hair, which might be due to invisible smaller hairs or other appendages (e.g. sweat ducts). Even given this uncertainty, our results show that H_2O_2 penetration through skin is dominated by the hair follicle pathway. This strongly favours the argument that permeation of hydrophilic molecules via the hair follicle pathway is substantial and should be targeted by epidermal sensing [17, 52–54].

To reinforce the statement that H_2O_2 preferentially penetrates skin through hair follicles, the permeability experiments were performed using full-thickness skin (4 mm thick). The same blue dot pattern in the H_2O_2 -sensitive PW microparticle layer developed (Fig. 5c). This confirms that the observed H_2O_2 penetration pattern is not due to dermatome-induced holes during preparation of thinner (0.5 mm) skin membranes.

Additionally, micrometre-sized particles (< 10 μm) can enter the follicular orifices [55]; hence, the PW particles, with an average size of 4.4 μm ± 1.2 μm (mean ± SD), may be localised inside the hair orifice/follicles, contributing to the development of the dot-like blue colour patterns observed during H_2O_2 penetration assays. In such a case, H_2O_2 penetrating the skin initially will meet PW particles lodged inside the hair follicle, explaining the observed blue dot pattern. As can be seen in Fig. 2b, after lipid extraction, no blue dot pattern was observed and H_2O_2 seems to cross the skin evenly/homogeneously. Additional experiments have also been done by first depositing a filter paper on the skin membrane and then pipetting a suspension of PW particles on the top of the filter. Similar dot-like patterns (data not shown) of PB appeared even for this H_2O_2 -sensing layer configuration. Altogether, the results strongly suggest that H_2O_2 has a strong preference to penetrate through the appendages of skin, particularly through hair follicles. This knowledge is important in the development of clinically robust epidermal sensing of H_2O_2 with micrometre resolution. Our

results show that micrometre resolution would allow faster biomarker detection: probably in 1–2 h as judged from the appearance of the first blue dots in Figs. 2 and 5.

Conclusions

This study aimed to visualise H₂O₂ penetration through skin membranes in order to model and rationalise strategies for the development of clinically relevant, epidermal sensing of ROS biomarkers, specifically H₂O₂. We conducted epidermal monitoring of H₂O₂ penetration through skin by using H₂O₂-sensitive Prussian white microparticles. The PW particle layer was deposited on the surface of skin membranes and after some time the PW particles turned blue, signalling H₂O₂ permeation through the skin. We found that PW particles with an average size of 4.4 μm ± 1.2 μm (mean ± SD) were sufficiently O₂-insensitive to allow prolonged (at least up to 24 h) epidermal monitoring of H₂O₂. The monitoring of H₂O₂ penetration was only possible after inhibition of skin catalase. Unfortunately, in most clinical cases, skin catalase inhibition will not be allowed; however, diseased skin is usually characterised by downregulation of catalase. Thus, epidermal sensing of H₂O₂ in clinically relevant situations might still be possible with a PW microparticle layer on the skin. Additionally, we found that the penetration of H₂O₂ through skin generates a blue dot pattern in the PW layer. About 74% ± 7% of the dots were associated with visible hair shafts. This observation, for the first time, firmly establishes that hair follicles are the dominant H₂O₂ penetration pathways in skin. In general, the results suggest that targeting hair follicles with micrometre resolution should provide more sensitive and rapid monitoring of low molecular weight, hydrophilic biomarkers of skin disorders. This is especially important to realise for development of epidermal sensing of H₂O₂. H₂O₂ is one of the common ROS, elevated in many inflammatory and autoimmune skin disorders, and its epidermal monitoring would be extremely valuable in managing these pathological conditions.

Acknowledgements Peter Falkman is acknowledged for obtaining SEM images. Zoltan Blum is acknowledged for reading and commenting the manuscript. TR and JE thank the Gustaf Th. Ohlsson Foundation.

Funding Open access funding provided by Malmö University. The authors received financial support from the Knowledge Foundation (20170058 and 20190010), the Swedish Research Council (2018-04320) and the Biofilms - Research Center for Biointerfaces at Malmö University.

Compliance with ethical standards

Conflict of interest The authors declare no competing financial interests. Bo Holmqvist and Anders Brinte are employed at ImaGene-iT stock company.

Open Access This article is licensed under a Creative Commons Attribution 4.0 International License, which permits use, sharing, adaptation, distribution and reproduction in any medium or format, as long as you give appropriate credit to the original author(s) and the source, provide a link to the Creative Commons licence, and indicate if changes were made. The images or other third party material in this article are included in the article's Creative Commons licence, unless indicated otherwise in a credit line to the material. If material is not included in the article's Creative Commons licence and your intended use is not permitted by statutory regulation or exceeds the permitted use, you will need to obtain permission directly from the copyright holder. To view a copy of this licence, visit <http://creativecommons.org/licenses/by/4.0/>.

References

- Kim D-H, Lu N, Ma R, Kim Y-S, Kim R-H, Wang S, Wu J, Won SM, Tao H, Islam A, Yu KJ, T-i K, Chowdhury R, Ying M, Xu L, Li M, Chung H-J, Keum H, McCormick M, Liu P, Zhang Y-W, Omenetto FG, Huang Y, Coleman T, Rogers JA (2011) Epidermal electronics. *Science* (Washington, DC, U S) 333(6044):838–843. <https://doi.org/10.1126/science.1206157>
- Kim J, Banks A, Cheng H, Xie Z, Xu S, Jang K-I, Lee JW, Liu Z, Gutruf P, Huang X, Wei P, Liu F, Li K, Dalal M, Ghaffari R, Feng X, Huang Y, Gupta S, Paik U, Rogers JA (2015) Epidermal electronics with advanced capabilities in near-field communication. *Small* 11(8):906–912. <https://doi.org/10.1002/sml.201402495>
- Krishnan SR, Su C-J, Xie Z, Patel M, Madhupathy SR, Xu Y, Freudman J, Ng B, Heo SY, Wang H, Ray TR, Leshock J, Stankiewicz I, Feng X, Huang Y, Gutruf P, Rogers JA (2018) Wireless, battery-free epidermal electronics for continuous, quantitative, multimodal thermal characterization of skin. *Small* 14(47):n/a. <https://doi.org/10.1002/sml.201803192>
- Zhu J, Zhou X, Kim H-J, Qu M, Jiang X, Lee KJ, Ren L, Wu Q, Wang C, Zhu X, Tebon P, Zhang S, Lee J, Ashammakhi N, Ahadian S, Dokmeci MR, Gu Z, Sun W, Khademhosseini A (2020) Gelatin methacryloyl microneedle patches for minimally invasive extraction of skin interstitial fluid. *Small* 16(16):1905910. <https://doi.org/10.1002/sml.201905910>
- Zhou T, Wang J-W, Huang M, Tan H, Wei H, Chen Z-D, Zhou T, Wang X, Liu X, Zhou T, Huang M, An R, Tan H, Zhou T, Wang F, He J, An R (2019) Breathable nanowood biofilms as guiding layer for green on-skin electronics. *Small* 15(31):e1901079
- Kim SB, Zhang Y, Won SM, Bhandokar AJ, Sekine Y, Xue Y, Koo J, Harshman SW, Martin JA, Park JM, Ray TR, Crawford KE, Lee K-T, Choi J, Pitsch RL, Grigsby CC, Strang AJ, Chen Y-Y, Xue Y, Kim J, Koh A, Ha JS, Huang Y, Kim SW, Rogers JA (2018) Super-absorbent polymer valves and colorimetric chemistries for time-sequenced discrete sampling and chloride analysis of sweat via skin-mounted soft microfluidics. *Small* 14(12):e1703334
- Heikenfeld J (2016) Technological leap for sweat sensing. *Nature* (London, U K) 529(7587):475–476. <https://doi.org/10.1038/529475a>
- Sonner Z, Wilder E, Gaillard T, Kasting G, Heikenfeld J (2017) Integrated sudomotor axon reflex sweat stimulation for continuous sweat analyte analysis with individuals at rest. *Lab Chip* 17(15):2550–2560. <https://doi.org/10.1039/C7LC00364A>
- Pandey PC, Shukla S, Skoog SA, Boehm RD, Narayan RJ (2019) Current advancements in transdermal biosensing and targeted drug delivery. *Sensors* 19(5):1028. <https://doi.org/10.3390/s19051028>
- Ullah S, Hamade F, Bubniene U, Engblom J, Ramanavicius A, Ramanaviciene A, Ruzgas T (2018) In-vitro model for assessing

- glucose diffusion through skin. *Biosens Bioelectron* 110:175–179. <https://doi.org/10.1016/j.bios.2018.03.039>
11. Cui B, Martin A, Mishra RK, Brunetti B, Nakagawa T, Dawkins TJ, Lyu M, Cristea C, Sandulescu R, Wang J (2018) Wearable wireless tyrosinase bandage and microneedle sensors: toward melanoma screening. *Adv Healthcare Mater* 7(7):n/a. <https://doi.org/10.1002/adhm.201701264>
 12. Darvishi S, Pick H, Lin T-E, Zhu Y, Li X, Ho P-C, Girault HH, Lesch A (2019) Tape-stripping electrochemical detection of melanoma. *Anal Chem* (Washington, DC, U S) 91(20):12900–12908. <https://doi.org/10.1021/acs.analchem.9b02819>
 13. De Guzman K, Morrin A (2017) Screen-printed tattoo sensor towards the non-invasive assessment of the skin barrier. *Electroanalysis* 29(1):188–196. <https://doi.org/10.1002/elan.201600572>
 14. Lin T-E, Bondarenko A, Lesch A, Pick H, Cortes-Salazar F, Girault HH (2016) Monitoring tyrosinase expression in non-metastatic and metastatic melanoma tissues by scanning electrochemical microscopy. *Angew Chem Int Ed* 55(11):3813–3816. <https://doi.org/10.1002/anie.201509397>
 15. Heikenfeld J, Jajack A, Feldman B, Granger SW, Gaitonde S, Begtrup G, Katchman BA (2019) Accessing analytes in biofluids for peripheral biochemical monitoring. *Nat Biotechnol* 37(4):407–419. <https://doi.org/10.1038/s41587-019-0040-3>
 16. Someya T, Amagai M (2019) Toward a new generation of smart skins. *Nat Biotechnol* 37(4):382–388. <https://doi.org/10.1038/s41587-019-0079-1>
 17. Lipani L, Dupont BGR, Doungmene F, Marken F, Tyrrell RM, Guy RH, Ilie A (2018) Non-invasive, transdermal, path-selective and specific glucose monitoring via a graphene-based platform. *Nat Nanotechnol* 13(6):504–511. <https://doi.org/10.1038/s41565-018-0112-4>
 18. Dallinger A, Keller K, Fitzek H, Greco F (2020) Stretchable and skin-conformable conductors based on polyurethane/laser-induced graphene. *ACS Appl Mater Interfaces* 12(17):19855–19865. <https://doi.org/10.1021/acsami.0c03148>
 19. Schallreuter KU, Moore J, Wood JM, Beazley WD, Gaze DC, Tobin DJ, Marshall HS, Panske A, Panzig E, Hibberts NA (1999) In vivo and in vitro evidence for hydrogen peroxide (H₂O₂) accumulation in the epidermis of patients with vitiligo and its successful removal by a UVB-activated pseudocatalase. *J Invest Dermatol Symp Proc* 4(1):91–96. <https://doi.org/10.1038/sj.jidsp.5640189>
 20. Guarrera M, Ferrari P, Rebora A (1998) Catalase in the stratum corneum of patients with polymorphic light eruption. *Acta Derm Venereol* 78(5):335–336
 21. Rabilloud T, Asselineau D, Miquel C, Calvayrac R, Darmon M, Vuillaume M (1990) Deficiency in catalase activity correlates with the appearance of tumor phenotype in human keratinocytes. *Int J Cancer* 45(5):952–956
 22. Hoffschir F, Daya-Grosjean L, Petit PX, Nocentini S, Dutrillaux B, Sarasin A, Vuillaume M (1998) Low catalase activity in xeroderma pigmentosum fibroblasts and SV40-transformed human cell lines is directly related to decreased intracellular levels of the cofactor, NADPH. *Free Radic Biol Med* 24(5):809–816. [https://doi.org/10.1016/S0891-5849\(97\)00350-X](https://doi.org/10.1016/S0891-5849(97)00350-X)
 23. Basu A, Devaraj S, Jialal I (2006) Dietary factors that promote or retard inflammation. *Arterioscler Thromb Vasc Biol* 26(5):995–1001. <https://doi.org/10.1161/01.ATV.0000214295.86079.d1>
 24. Myers A (2015) The autoimmune solution: prevent and reverse the full spectrum of inflammatory symptoms and diseases. Harper Collins, New York
 25. Hernandez AR, Boutonnet M, Svensson B, Butler E, Lood R, Blom K, Vallejo B, Anderson C, Engblom J, Ruzgas T, Bjoerklund S (2019) New concepts for transdermal delivery of oxygen based on catalase biochemical reactions studied by oxygen electrode amperometry. *J Control Release* 306:121–129. <https://doi.org/10.1016/j.jconrel.2019.06.001>
 26. Nagaraja S, Reifman J, Mitrophanov AY, Nagaraja S, Mitrophanov AY, Chen L, DiPietro LA (2019) Predictive approach identifies molecular targets and interventions to restore angiogenesis in wounds with delayed healing. *Front Physiol* 10:636
 27. Bjoerklund S, Andersson JM, Pham QD, Nowacka A, Topgaard D, Sparr E (2014) Stratum corneum molecular mobility in the presence of natural moisturizers. *Soft Matter* 10(25):4535–4546. <https://doi.org/10.1039/C4SM00137K>
 28. Nocchi S, Bjoerklund S, Svensson B, Engblom J, Ruzgas T (2017) Electrochemical monitoring of native catalase activity in skin using skin covered oxygen electrode. *Biosens Bioelectron* 93:9–13. <https://doi.org/10.1016/j.bios.2017.01.001>
 29. Bjoerklund S, Pham QD, Jensen LB, Knudsen NO, Nielsen LD, Ekelund K, Ruzgas T, Engblom J, Sparr E (2016) The effects of polar excipients transcutool and dexpanthenol on molecular mobility, permeability, and electrical impedance of the skin barrier. *J Colloid Interface Sci* 479:207–220. <https://doi.org/10.1016/j.jcis.2016.06.054>
 30. Hu M, Jiang JS (2011) Facile synthesis of air-stable Prussian white microcubes via a hydrothermal method. *Mater Res Bull* 46(5):702–707. <https://doi.org/10.1016/j.materresbull.2011.01.017>
 31. Pearce J (1994) Studies of any toxicological effects of Prussian blue compounds in mammals—a review. *Food Chem Toxicol* 32(6):577–582. [https://doi.org/10.1016/0278-6915\(94\)90116-3](https://doi.org/10.1016/0278-6915(94)90116-3)
 32. Roberts L (1987) Radiation accident grips Goiania. *Science* 238(4830):1028–1031
 33. Mosshammer M, Kuehl M, Koren K (2017) Possibilities and challenges for quantitative optical sensing of hydrogen peroxide. *Chemosensors* 5(4):28/21–28/23. <https://doi.org/10.3390/chemosensors5040028>
 34. Chu Z, Liu Y, Jin W (2017) Recent progress in Prussian blue films: methods used to control regular nanostructures for electrochemical biosensing applications. *Biosens Bioelectron* 96:17–25. <https://doi.org/10.1016/j.bios.2017.04.036>
 35. Mitragotri S, Anissimov YG, Bunge AL, Frasca HF, Guy RH, Hadgraft J, Kasting GB, Lane ME, Roberts MS (2011) Mathematical models of skin permeability: an overview. *Int J Pharm* 418(1):115–129. <https://doi.org/10.1016/j.ijpharm.2011.02.023>
 36. Hellemans L, Corstjens H, Neven A, Declercq L, Maes D (2003) Antioxidant enzyme activity in human stratum corneum shows seasonal variation with an age-dependent recovery. *J Invest Dermatol* 120(3):434–439. <https://doi.org/10.1046/j.1523-1747.2003.12056.x>
 37. Eskandari M, Rembiesa J, Startaite L, Holefors A, Valanciute A, Faridbod F, Ganjali MR, Engblom J, Ruzgas T (2019) Polyphenol-hydrogen peroxide reactions in skin: in vitro model relevant to study ROS reactions at inflammation. *Anal Chim Acta* 1075:91–97. <https://doi.org/10.1016/j.aca.2019.05.032>
 38. Otberg N, Richter H, Knuttel A, Schaefer H, Sterry W, Lademann J (2004) Laser spectroscopic methods for the characterization of open and closed follicles. *Laser Phys Lett* 1(1):46–49. <https://doi.org/10.1002/lapl.200310011>
 39. Jepps OG, Dancik Y, Anissimov YG, Roberts MS (2013) Modeling the human skin barrier - towards a better understanding of dermal absorption. *Adv Drug Deliv Rev* 65(2):152–168. <https://doi.org/10.1016/j.addr.2012.04.003>
 40. Karyakin AA (2001) Prussian blue and its analogues: electrochemistry and analytical applications. *Electroanalysis* 13(10):813–819. [https://doi.org/10.1002/1521-4109\(200106\)13:10<813::AID-ELAN813>3.0.CO;2-Z](https://doi.org/10.1002/1521-4109(200106)13:10<813::AID-ELAN813>3.0.CO;2-Z)
 41. Li M, Zhao G, Yue Z, Huang S (2009) Sensor for traces of hydrogen peroxide using an electrode modified by multiwalled carbon nanotubes, a gold-chitosan colloid, and Prussian blue. *Microchim*

- Acta 167(3–4):167–172. <https://doi.org/10.1007/s00604-009-0238-z>
42. Yang J, Lin M, Cho MS, Lee Y (2015) Determination of hydrogen peroxide using a Prussian blue modified macroporous gold electrode. *Microchim Acta* 182(5–6):1089–1094. <https://doi.org/10.1007/s00604-014-1433-0>
 43. Cheng Z, Shen Q, Yu H, Han D, Zhong F, Yang Y (2017) Non-enzymatic sensing of hydrogen peroxide using a glassy carbon electrode modified with the layered MoS₂-reduced graphene oxide and Prussian blue. *Microchim Acta* 184(12):4587–4595. <https://doi.org/10.1007/s00604-017-2503-x>
 44. Lee S-H, Huh Y-D (2012) Preferential evolution of Prussian blue's morphology from cube to hexapod. *Bull Kor Chem Soc* 33(3):1078–1080. <https://doi.org/10.5012/bkcs.2012.33.3.1078>
 45. Yang J, Wang H, Lu L, Shi W, Zhang H (2006) Crystal growth & design. *Growth (Lakeland)*:10–12. <https://doi.org/10.1021/cg060469r>
 46. Koren K, Jensen PO, Kuhl M (2016) Development of a rechargeable optical hydrogen peroxide sensor - sensor design and biological application. *Analyst (Cambridge, U K)* 141(14):4332–4339. <https://doi.org/10.1039/C6AN00864J>
 47. Lademann J, Richter H, Schanzer S, Knorr F, Meinke M, Sterry W, Patzelt A (2011) Penetration and storage of particles in human skin: perspectives and safety aspects. *Eur J Pharm Biopharm* 77(3):465–468. <https://doi.org/10.1016/j.ejpb.2010.10.015>
 48. Ponc M (1981) Mechanism of percutaneous absorption. *Pharm Weekbl* 116(49):1502–1508
 49. Teichmann A, Jacobi U, Ossadnik M, Richter H, Koch S, Sterry W, Lademann J (2005) Differential stripping: determination of the amount of topically applied substances penetrated into the hair follicles. *J Invest Dermatol* 125(2):264–269. <https://doi.org/10.1111/j.0022-202X.2005.23779.x>
 50. Meidan VM, Bonner MC, Michniak BB (2005) Transfollicular drug delivery-is it a reality? *Int J Pharm* 306(1–2):1–14. <https://doi.org/10.1016/j.ijpharm.2005.09.025>
 51. Grams YY (2005) Influence of molecular properties and delivery system design on the transfollicular transport across the skin. Doctoral thesis, Leiden University, Leiden
 52. Horita D, Todo H, Sugibayashi K (2014) Analysis of the pretreatment effect of ethanol on the stratum corneum- and hair follicular-penetration of drugs using the hair follicle-plugging method. *Chem Pharm Bull* 62(6):578–585. <https://doi.org/10.1248/cpb.c14-00096>
 53. Mohd F, Todo H, Yoshimoto M, Yusuf E, Sugibayashi K (2016) Contribution of the hair follicular pathway to total skin permeation of topically applied and exposed chemicals. *Pharmaceutics* 8(4):32/31–32/12. <https://doi.org/10.3390/pharmaceutics8040032>
 54. Otberg N, Teichmann A, Rasuljev U, Sinkgraven R, Sterry W, Lademann J (2007) Follicular penetration of topically applied caffeine via a shampoo formulation. *Skin Pharmacol Physiol* 20(4):195–198. <https://doi.org/10.1159/000101389>
 55. Toll R, Jacobi U, Richter H, Lademann J, Schaefer H, Blume-Peytavi U (2004) Penetration profile of microspheres in follicular targeting of terminal hair follicles. *J Invest Dermatol* 123(1):168–176. <https://doi.org/10.1111/j.0022-202X.2004.22717.x>

Publisher's note Springer Nature remains neutral with regard to jurisdictional claims in published maps and institutional affiliations.